10748 *Inorg. Chem.* **2009**, *48*, 10748–10756
DOI: 10.1021/ic9015299

Inorganic Chemistry
Article

High Energy Resolution X-ray Absorption Spectroscopy of Environmentally Relevant Lead(II) Compounds

Janine C. Swarbrick,*,† Ulf Skyllberg,‡ Torbjörn Karlsson,§ and Pieter Glatzel*,†

†*European Synchrotron Radiation Facility (ESRF), BP 220, F-38043, Grenoble, Cedex 9, France,* ‡*Swedish University of Agricultural Sciences, Department of Forest Ecology and Management, SE-90183, Umeå, Sweden, and* §*Umeå University, Department of Chemistry, SE-90187, Umeå, Sweden*

Received August 1, 2009

The determination of the chemical environment of Pb in natural samples is a challenge of great importance in environmental and health physics. We report a high energy resolution fluorescence detection (HERFD) X-ray absorption near-edge spectroscopy (XANES) study at the Pb L_3 and L_1 absorption edges to determine the chemical environment of Pb in a series of model and environmentally relevant compounds. HERFD spectroscopy can reveal increased spectral detail due to an apparent reduction in the core hole lifetime broadening. HERFD spectra of model Pb(II) compounds were compared to FEFF 8.4 multiple scattering calculations with reduced peak broadening parameters, and density of state (DOS) simulations, to determine the origins of the spectral features. A pre-edge in the L_3 XANES is revealed which is shown to arise from hybridization between the Pb *p* and *d* states. HERFD spectra of Pb(II)-containing environmentally relevant solutions were compared to model spectra and calculations. The results presented in this paper show that the chemical environment of Pb can be identified from spectral features resolved in HERFD spectroscopy at the Pb L_3 edge. The technique provides information that is complementary to conventional extended X-ray absorption fine structure (EXAFS) spectroscopy.

Introduction

Understanding Pb coordination is of paramount importance in environmental studies.[1] Divalent lead (Pb(II)) is a widespread trace element in soils, sediments, waters and atmospheric pollutants. The highly toxic effect of Pb(II) is believed to be caused by its high binding affinity for thiol and phosphate groups in enzymes, proteins and cell-membranes.[2] At oxidative conditions and neutral pH, complexation to various oxygen containing inorganic ligands such as phosphates, carbonates and hydroxyls, as well as halides and organic ligands dominate the chemical speciation of Pb(II) in the environment. In low molecular mass (LMM) organic ligands, Pb(II) binds mainly to oxygen, nitrogen and sulfur functional groups, whereas the identity of Pb(II) ligands in macromolecules such as natural organic matter is less well studied.[3] The high-affinity of the Pb^{2+} ion for oxygen functional groups at surfaces of iron(III)-oxyhydroxides, as compared to other trace metals, is well-known (e.g.[4]), whereas organic ligands and sulfides compete for Pb(II) under anoxic conditions.[5] Childhood lead poisoning,[6] crop poisoning,[7] and pollution by atmospheric Pb species[8,9] are growing health issues in polluted regions and require the identification of Pb species in different complexes.

Extended X-ray absorption fine structure (EXAFS) spectroscopy has been used in studies of Pb speciation in soils, plants and microorganisms.[10−13] Because of a stereochemical

*E-mail: janine.grattage@esrf.fr (J.C.S.); glatzel@esrf.fr (P.G.).

(1) Davidovich, R. L.; Stavila, V.; Marinin, D. V.; Voit, E. I.; Whitmire, K. H. *Coord. Chem. Rev.* **2009**, *253*, 1316–1352.
(2) Abu-Dari, K.; Hahn, F. E.; Raymond, K. N. *J. Am. Chem. Soc.* **1990**, *112*, 1519–1524.
(3) Xia, K.; Bleam, W.; Helmke, P. A. *Geochim. Cosmochim. Acta* **1997**, *61*, 2211–2221.
(4) Weng, L.; Temminghoff, E. J. M.; van Riemsdijk, W. H. *Environ. Sci. Technol.* **2001**, *35*, 4436–4443.
(5) Taillefert, M.; Lienemann, C. P.; Gaillard, J. F.; Perret, D. *Geochim. Cosmochim. Acta* **2000**, *64*, 169–183.
(6) Magyar, J. S.; Weng, T. C.; Stern, C. M.; Dye, D. F.; Rous, B. W.; Payne, J. C.; Bridgewater, B. M.; Mijovilovich, A.; Parkin, G.; Zaleski, J. M.; Penner-Hahn, J. E.; Godwin, H. A. *J. Am. Chem. Soc.* **2005**, *127*, 9495–9505.
(7) Wang, H. H.; Shan, X. Q.; Liu, T.; Xie, Y. N.; Wen, B.; Zhang, S. Z.; Han, F.; van Genuchten, M. T. *Planta* **2007**, *225*, 1483–1494.
(8) Matzapetakis, M.; Ghosh, D.; Weng, T. C.; Penner-Hahn, J. E.; Pecoraro, V. L. *J. Biol. Inorg. Chem.* **2006**, *123*, 876–890.
(9) Tan, M. G.; Zhang, G. L.; Li, X. L.; Zhang, Y. X.; Yue, W. S.; Chen, J. M.; Wang, Y. S.; Li, A. G.; Li, Y.; Zhang, Y. M.; Shan, Z. C. *Anal. Chem.* **2006**, *78*, 8044–8050.
(10) Manceau, A.; Boisset, M. C.; Sarret, G.; Hazemann, J. L.; Mench, M.; Cambier, P.; Prost, R. *Environ. Sci. Technol.* **1996**, *30*, 1540–1552.
(11) Sarret, G.; Manceau, A.; Cuny, D.; van Haluwyn, C.; Déruelle, S.; Hazemann, J. L.; Soldo, Y.; Eybert-Bérard, L.; Menthonnex, J. J. *Environ. Sci. Technol.* **1998**, *32*, 3325–3330.
(12) Fomina, M.; Charnock, J.; Bowen, A. D.; Gadd, G. M. *Environ. Microbiol.* **2007**, *9*, 308–321.
(13) Sarret, G.; Vangronsveld, J.; Manceau, A.; Musso, M.; D'Haen, J.; Menthonnex, J. J.; Hazemann, J. L. *Environ. Sci. Technol.* **2001**, *35*, 2854–2859.

 Published on Web 10/19/2009

influence of the lone electron pair in the outer-shell (Pb(II) has a $5d^{10}6s^2$ electronic structure), the coordination geometries of Pb(II) are often complex (holo- or hemidirected) and asymmetric. The number of possible ligands varies; a high coordination number of up to 12 oxygen donor ligands is possible, as is a low coordination number of nitrogen donor ligands, with 4−6 donor O/N/S atoms in the most common structures.[14] The complex coordination chemistry of Pb(II), combined with a high static and dynamic disorder results in smeared-out spectral features, and makes it difficult to obtain higher-shell structural data from conventional Pb EXAFS analysis.[10] Thus, other spectroscopic techniques need to be developed if the coordination chemistry of Pb(II) is to be understood in complex matrices such as natural organic matter and biological samples.

With the increase in the number of synchrotron radiation sources worldwide, the use of synchrotron based techniques is now a viable option for more and more researchers in various research fields. A commonly used technique for studying the oxidation state and chemical coordination of atoms in dilute samples is fluorescence detected XANES, which is often achieved using a Ge detector or photodiode to measure the fluorescence photons emitted. Ge detectors have an energy resolution of 0.05,[15] whereas photodiodes have no energy resolution. To resolve spectral features unique to a particular compound or chemical environment which can act as a chemical fingerprint, rather than simply observing a shift in the absorption edge, an X-ray analyzer using perfect crystal Bragg optics may be used. The experimental broadening in such a setup is greatly reduced and a spectral resolution can be achieved that is below the core hole lifetime broadening.[16−18] This high resolution approach is particularly useful in studying heavier elements such as Pb which do not show fine structural details in conventional XANES.[19,20] Due to the reduced efficiency of emitted photon capture, an intense photon source is required for the technique, namely a third-generation synchrotron.

In this paper we describe the use of HERFD spectroscopy in studying Pb compounds to measure characteristic spectral features from different Pb chemical environments, and to compare these measurements with FEFF calculations of the HERFD spectra and the Pb density of states (DOS) to determine the origin of different spectral features. For three model samples (Figure 1) a full resonant inelastic X-ray scattering (RIXS) 2D plane was measured by recording the L_3 edge XANES spectra over a range of energies covering the $L\beta_5$ X-ray emission line. It is important to ensure the equivalence of transitions being recorded in HERFD compared with conventional XANES by recording a full RIXS plane and noting the absence of additional peaks away from the HERFD

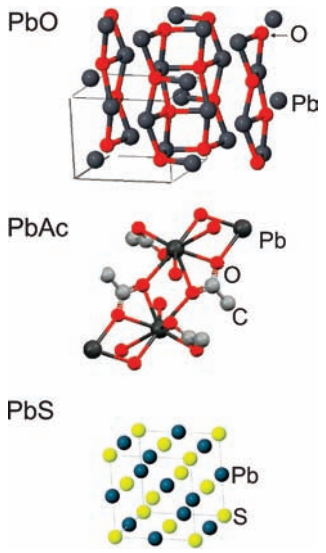

Figure 1. Schematic diagrams of the crystal structures used for FEFF calculations of PbO, PbAc ($Pb(O_2C_2H_3)_2 \cdot 3H_2O$), and PbS.

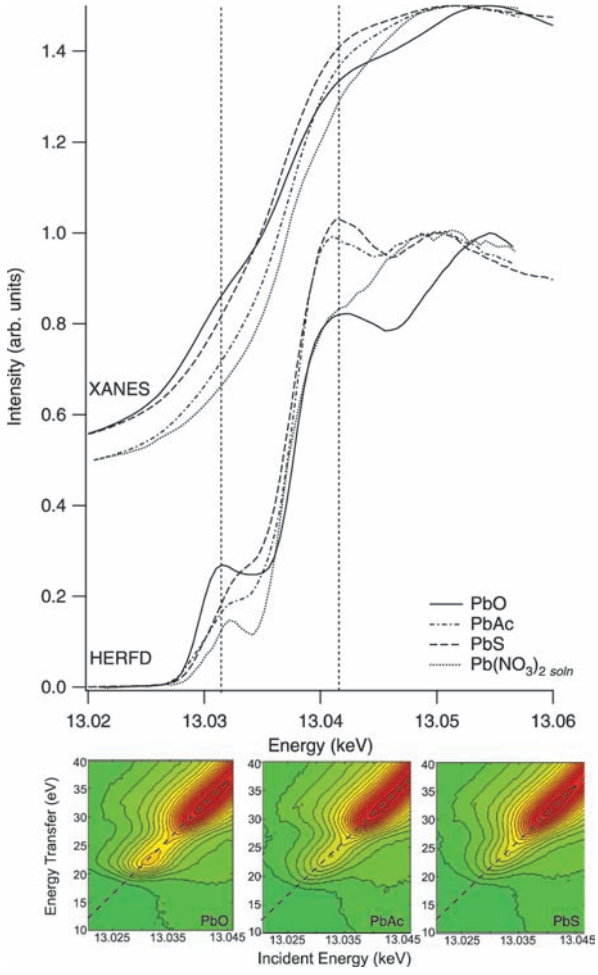

Figure 2. Comparison of Pb L_3 edge XANES and HERFD measurements for the standard compounds PbO, $Pb(NO_3)_2$, PbAc, and PbS, and full 2D RIXS planes over the $L\beta_5$ emission line for PbO, PbAc, and PbS.

diagonal (see Figure 2). We show that characteristic features for each compound can be resolved using HERFD, thus providing a fingerprint for Pb within different chemical environments. Previously reported preliminary HERFD

(14) Shimony-Livny, L.; Glusker, J. P.; Bock, C. W. *Inorg. Chem.* **1998**, *37*, 1853–1867.
(15) Glatzel, P.; de Groot, F. M. F.; Manoilova, O.; Grandjean, D.; Weckhuysen, B. M.; Bergmann, U.; Barrea, R. *Phys. Rev. B: Condens. Matter* **2005**, *72*, 014117.
(16) Glatzel, P.; Bergmann, U. *Coord. Chem. Rev.* **2005**, *249*, 65–95.
(17) Hayashi, H.; Takeda, R.; Udagawa, Y.; Nakamura, T.; Miyagawa, H.; Shoji, H.; Nanao, S.; Kawamura, N. *Phys. Rev. B: Condens. Matter* **2003**, *68*, 045122.
(18) Hämäläinen, K.; Siddons, D. P.; Hastings, J. B.; Berman, L. E. *Phys. Rev. Lett.* **1991**, *67*, 2850–2853.
(19) Safonova, O. V.; Tromp, M.; van Bokhoven, J. A.; de Groot, F. M. F.; Evans, J.; Glatzel, P. *J. Phys. Chem. B* **2006**, *110*, 16162–16164.
(20) Welter, E.; Calmano, W.; Mangold, S.; Tröger, L. *Fresenius J. Anal. Chem.* **1999**, *364*, 238–244.

studies at the Pb L_3 edge show encouraging enhancements in spectral detail.[21] This paper builds upon previous work to give a systematic characterization of model crystalline and metalloorganic Pb compounds. We also measured HERFD spectra at the Pb L_1 absorption edge, where increased resolution is achieved using HERFD although little additional detail is revealed compared with standard XANES. We show that the spectra from model powder Pb compounds can be simulated using the FEFF 8.4 multiple scattering code with reduced broadening parameters to mimic the effective reduction in the experimental broadening observed using HERFD. From these calculations we show the contribution of the Pb *p* DOS and *d* DOS to the L_1 and L_3 absorption edges.

Method

X-ray Emission and Absorption Measurements. Experiments were performed on beamline ID26 at the European Synchrotron Radiation Facility. The electron energy was 6.0 GeV with a ring current of between 170 mA and 200 mA. The incident energy was selected by using the ⟨111⟩ reflection of a pair of cryogenically cooled Si single crystals. Higher harmonics were suppressed using two mirrors with a Pd/Cr coating at 3 mrad. The beam size was approximately 0.3 mm horizontal and 1 mm vertical. The analyzer used exploits the Bragg reflection of a spherically bent crystal with 1 m bending radius in the horizontal Rowland geometry: Si(880) was used for detecting the Lβ_5 emission line (13.014 keV) and Si(951) for the Lβ_4 emission line (12.307 keV). We recorded the intensity variation of the Lβ_5 (Lβ_4) line as a function of the incident energy to record high-resolution absorption spectra at the Pb L_3 (L_1) edges at 13.035 keV (15.861 keV). The emitted photons were measured using an 200 μm avalanche photodiode (APD). Pb L_3 edge (probing $2p_{3/2} \rightarrow nd$, $n \geq 6$ transitions) HERFD spectra were recorded for the Pb compounds over an incident energy range of 13.01−13.10 keV for solid samples and between 13.021−13.057 keV for solution samples. L_1 edge spectra of the solid samples (probing $2s \rightarrow np$, $n \geq 6$ transitions) were recorded between 15.82−15.94 keV. Full 2-D RIXS planes for the solid model compounds were recorded by measuring the Pb L_3 absorption edge over a range of emission energies spanning the Lβ_5 line. The energy bandwidth in the incident energy is 1.9 (2.3) eV at the L_3 (L_1) edge, and the combined energy bandwidth (incident convoluted with emission energy bandwidth) is 3.0 (3.5) eV using the Lβ_5 (Lβ_4) line.

The core hole lifetime broadenings of the intermediate and final states determine the overall spectral broadening seen in HERFD spectra, as determined from the formula given by de Groot et al.[22] as

$$\Gamma_{APP} = 1/\sqrt{1/(\Gamma_{INT})^2 + 1/(\Gamma_{FIN})^2} \quad (1)$$

where Γ_{APP}, Γ_{INT}, and Γ_{FIN} are the apparent, intermediate, and final state lifetime broadenings, respectively. As well as inherent core hole lifetime broadening, it is necessary to include the instrumental broadening or energy bandwidth. In this case the overall bandwidth E_{TOT} is 3.0 (3.5) eV, which is a combination of the incident (E_{INC}) and emission (E_{EMI}) energy bandwidths, related by the expression $E_{TOT} = \sqrt{E_{INC}^2 + E_{EMI}^2}$. E_{INC} is determined as the incident energy divided by the resolving power of the monochromator (7000 in this case). The formula for the approximate broadening of the Voigt-type profile peak f_V obtained by convoluting the Gaussian-type profile broadening f_G with the Lorenzian-type profile broadening f_L is[23]

$$f_V = 0.5346 f_L + \sqrt{0.2169 f_L^2 + f_G^2} \quad (2)$$

Table 1. Core Hole Lifetime Broadenings of the Intermediate (Γ_{INT}) and Final (Γ_{FIN}) States Used To Record the Pb L_1 and L_3 Edges[a]

Emission line	M_5 (Lα_1)	$O_{4,5}$ (Lβ_5)	M_2 (Lβ_4)	
Edge	L_3 ($2p_{3/2}$)	L_3 ($2p_{3/2}$)	L_1 ($2s$)	
Γ_{INT}	5.8	5.8	12.2	12.2
Γ_{FIN}	2.8	0.4	7.0	15.0[b]
E_{INC}	1.9	1.9	2.3	2.3
E_{EMI}	2.4	2.4	2.7	2.7
$\Gamma_{FIN} * E_{EMI} = \Gamma_1$(*eq* 2)	4.2	2.6	8.0	15.5
$\Gamma_1 * E_{EMI} = \Gamma_1$(*eq* 2)	3.4	2.4	6.7	9.6
$\Gamma_2 * E_{INC} = \Gamma_{TOT}$(*eq* 2)	**4.3**	**3.4**	**7.4**	**10.1**

[a] The total overall spectral broadening Γ_{TOT} is calculated using the instrumental broadening of the incident energy (E_{INC}) and the emitted energy (E_{EMI}). The total instrumental broadening is 3.0 eV at the L_3 edge and 3.5 eV at the L_1 edge. [b] Γ_{FIN} for the M_2 line is not available in the literature; the number here is estimated to be 7 eV from extrapolation from available data in the literature[24] and is given in the FEFF calculations as 15 eV, thus both values are included.

We estimate the overall spectral broadening in three steps. First we convolute the final state lifetime broadening Γ_{FIN} with the emission energy bandwidth E_{EMI} using eq 2. We use this value in eq 1 as the final state broadening and determine the broadening including the contribution from the intermediate core hole lifetime broadening Γ_{INT} . Finally we include the effect of the incident energy bandwidth, E_{INC}, again using eq 2. Table 1 gives the core hole lifetime broadening of the intermediate and final states for the spectra presented here,[24] with the experimental broadening factors. The estimated overall peak broadening Γ_{TOT} is calculated using the method above. For comparison the Lα_1 line figures are included as used by Izumi et al.[21] to record the Pb L_3 edge. Using the Lβ_5 line we further reduce the lifetime broadening effects at the Pb L_3 edge compared with using the Lα_1 line and thus achieve an overall improvement of the spectral resolution, which is in fact dominated by the experimental bandwidth.

The model lead compounds chosen for study were powders of PbO (massicot, orthorhombic β-PbO), Pb acetate ([Pb(CH_3-COO)$_2 \cdot 3H_2O$], abbreviated in this paper as PbAc), PbS(galena), and a 40 mM $Pb(NO_3)_2$ aqueous solution (dominated by >95% hydrated Pb^{2+} ions). These model compounds were selected to provide different Pb-ligand systems, including O, C, S, and Pb^{2+} ions in solution. The powder Pb compounds (PbO, PbAc, PbS) were diluted with boronitride and pressed into pellets for mounting at the beamline. Model aqueous phase compounds were prepared by adding Pb(II) (from a 150 mM Pb(II)-nitrate solution) to different organic ligands relevant for natural waters and soils, namely glycine (PbGly), cysteine (PbCys), histidine (PbHist), and desferrioxamine-B (a siderophore, PbDFO-B). The final concentration of Pb was 40 mM. The ligand concentration and pH were adjusted in order to (when reliable thermodynamic data were available) produce one dominant species as well as providing a good signal-to-noise ratio for XAS analyses. The pH was adjusted to 10.4 in PbGly (resulting in >95% $Pb(Gly)_2$ complexes, as verified by EXAFS) and to 7.7 in PbCys (predominance of PbCys), PbDFO-B, and PbHist (compositions unclear). In all solutions some precipitation occurred, indicating that both dissolved and colloidal forms of Pb-complexes were formed. Measured count rates were determined for the Lβ_5 line to be 40,000 counts/s for concentrated pellet samples

(21) Izumi, Y.; Nagamori, H.; Kiyotaki, F.; Masih, D.; Minato, T.; Roisin, E.; Candy, J.; Tanida, H.; Uruga, T. *Anal. Chem.* **2005**, *77*, 6969–6975.

(22) de Groot, F. M. F.; Krisch, M. H.; Vogel, J. *Phys. Rev. B: Condens. Matter* **2002**, *66*, 195112.

(23) Olivero, J. J.; Longbothum, R. L. *J. Quant. Spectrosc. Radiat. Transfer* **1977**, *17*, 233–236.

(24) *Unoccupied Electronic States: Fundamentals of XANES, EELS, IPS and BIS*; Fuggle, J. C., Inglesfield, J. E., Eds.; Springer, Berlin, 1992; Vol. 69, Appendix B.

and 1600 counts/s for the diluted solutions. The beamline is capable of measuring low levels of Pb in an organic matrix down to $<0.1\%$ or 1 mM, with an excellent signal-to-noise ratio of $>95\%$ (the background counts are <5 counts/s). The experiments here were performed using one analyzer crystal, but it is possible to increase the solid angle by a factor of up to 20 times, by adding extra analyzer crystals and reducing the bending radius, to further improve the count rate. The measurements can also be made from various bulk sample environments, such as soils and liquids, making the technique ideal for the study of natural Pb-containing matter. The samples were checked for radiation damage prior to measuring spectra by recording the absorption edge region using a photodiode (for the highest detection efficiency), and the time taken until a change was seen between two consecutive spectra was taken as the time limit after which radiation damage occurs. All the spectra were then recorded on fresh sample spots for a time less than this radiation damage time limit.

Calculations. FEFF8.4[25,26] was used to model the measured HERFD spectra and to determine the Pb DOS contributions to the spectra. The code employs full multiple scattering (FMS) and the muffin-tin (MT) approximation for wave function expansion, to determine a periodic potential and calculate the absorption spectrum for the scattering atom. FEFF calculations were performed using a self-consistent field (SCF) approximation within a 5 Å radius of the central Pb atom and include both dipole and quadrupole contributions. In fact the inclusion of the quadrupole component has a negligible effect on the calculated spectra which are dominated by dipole transitions. The calculations were performed both with and without the NOHOLE card to assess the effect of the core hole. Little difference was found between the two cases; the presented spectra include the NOHOLE approximation. The Hedin-Lundqvist self-energy correction was employed. The high energy resolution was modeled by reducing the spectral broadening in FEFF using the EXCHANGE card (using -5.0 for the L_3 edge and -4.2 for the L_1 edge). This EXCHANGE parameter reduced the tabulated broadening value applied to the calculated spectra by -5 eV (-4.2 eV). Spectra calculated for comparison with standard XANES (total fluorescent yield, or TFY) used the default EXCHANGE card parameters.

The crystal structures were taken from the current literature and are shown in Figure 1: PbO (massicot),[27] PbAc ($Pb(O_2C_2H_3)_2\cdot 3H_2O$),[28] and PbS (galena).[29] The Amsterdam Density Functional code (ADF[30]) was used to model molecular species. A single Pb^{2+} ion surrounded by eight water molecules[31] was modeled to represent a Pb(II) ion in solution in likely coordination geometries, with Pb−O bond distances constrained to 2.49 Å per Rouff et al.[32] ADF was also used to model molecular species for PbGly and PbCys using bond distances obtained from EXAFS measurements.[33]

Results

Pb L_3 Absorption Edge. Figure 2 shows the standard XANES and HERFD data for the model compounds PbO, PbAc, and PbS as well as $Pb(NO_3)_2$ in solution. The RIXS planes are also given for the solid samples. Due to the increased detail obtained, the HERFD spectra are easily distinguishable for each compound and thus are much more useful for identifying a particular compound,[35] conversely it is difficult to identify distinct features unique to a particular compound in standard XANES. The PbAc XANES spectrum is similar to that previously reported for $Pb(CH_3COO)_2\cdot 3H_2O$.[34] Some differences among the samples are apparent in both the XANES and HERFD, for example the higher pre-edge intensity for PbO and lower pre-edge intensity for $Pb(NO_3)_{2sol}$ can be observed using both techniques. The lower intensity for PbO and $Pb(NO_3)_{2sol}$ spectra at 13.046 keV compared with the other two compounds is apparent in both measurements. Also the energy of the absorption edge follows the same trend in both XANES and HERFD spectra as far as discernible. It can be seen that the PbO spectrum in particular has the most intense pre-edge and has a post-edge maximum shifted to higher energies compared with the other samples, at 13.054 keV rather than 13.050 keV. Also for the PbS sample, it can be seen that there is a pre-edge feature which is not a distinct peak but is less separated from the main edge than for the other samples.

Comparison of HERFD spectra with the full 2D RIXS planes confirms that measuring the absorption edges using the high resolution method with a crystal analyzer does not include any extra information, or remove information recorded in standard XANES, as there are no additional peaks away from the diagonal cut (which would represent additional electronic transitions). Therefore the HERFD line scan spectra in Figure 2 represent the same transitions as those probed in standard XANES. HERFD spectra are partial fluorescence yield (PFY) spectra which record one type of secondary process, and the signal may not be proportional to the absorption cross section.[36] However, it can be seen that the PFY are a good approximation to the absolute cross section here since the same features seen in the XANES are also seen in the HERFD, as described above. The main difference between the HERFD and XANES in this case is the apparent reduction in lifetime broadening in the high resolution spectra, allowing the identification of spectral features unique to each particular compound.

Pb L_3 Edge FEFF Calculations. The apparent reduction in lifetime broadening to enhance spectral details can be modeled using FEFF calculations as shown in Figure 3, which compares the measured and calculated Pb L_3 edge HERFD spectra for each model compound. The calculated spectrum for solid PbO shows three main peaks at the same energies as peaks in the HERFD measurements, at 13.032 keV, 13.042 keV, and 13.054 keV. A calculation with standard broadening is also shown for PbO, compared with the TFY XANES measurement. The PbO calculations for HERFD and TFY XANES show a lower spectral intensity before 13.054 keV (all spectra have been

(25) Ankudinov, A.; Ravel, B.; Rehr, J.; Conradson, S. *Phys. Rev. B: Condens. Matter* **1998**, *58*, 7565–7576.
(26) Rehr, J. J.; Albers, R. C. *Rev. Mod. Phys.* **2000**, *73*, 621–654.
(27) Hill, R. J. *Acta Crystallogr., Sect. C: Cryst. Struct. Commun.* **1985**, *64*, 1281–1284.
(28) Bryant, R. G.; Chacko, V. P.; Etter, M. C. *Inorg. Chem.* **1984**, *23*, 3580–3584.
(29) Noda, Y.; Matsumoto, K.; Ohba, S.; Saito, Y.; Toriumi, K.; Iwata, Y.; Shibuya, I. *Acta Crystallogr., Sect. C: Cryst. Struct. Commun.* **1987**, *43*, 1443–1445.
(30) Guerra, C. F.; Snijders, J. G.; te Velde, G.; Baerends, E. J. *Theor. Chem. Acc.* **1998**, *99*, 391–403.
(31) Wander, M. F. C.; Clark, A. E. *Inorg. Chem.* **2008**, *47*, 8233–8241.
(32) Rouff, A.; Elzinga, E. J.; Reeder, R. J. *Environ. Sci. Technol.* **2006**, *40*, 1792–1798.
(33) Skyllberg, U. Manuscript in preparation.
(34) Izumi, Y.; Kiyotaki, F.; Seida, Y. *J. Phys. Chem. B* **2002**, *106*, 1518–1520.
(35) Funasaka, K.; Tojo, T.; Katahira, K.; Shinya, M.; Miyazaki, T.; Kamiura, T.; Yamamoto, O.; Moriwaki, H.; Tanida, H.; Takaoka, M. *Sci. Total Environ.* **2009**, *403*, 230–234.
(36) de Groot, F. M. F.; Arrio, M. A.; Sainctavit, Ph.; Cartier, Ch.; Chen, C. H. *Solid State Commun.* **1994**, *92*, 991–995.

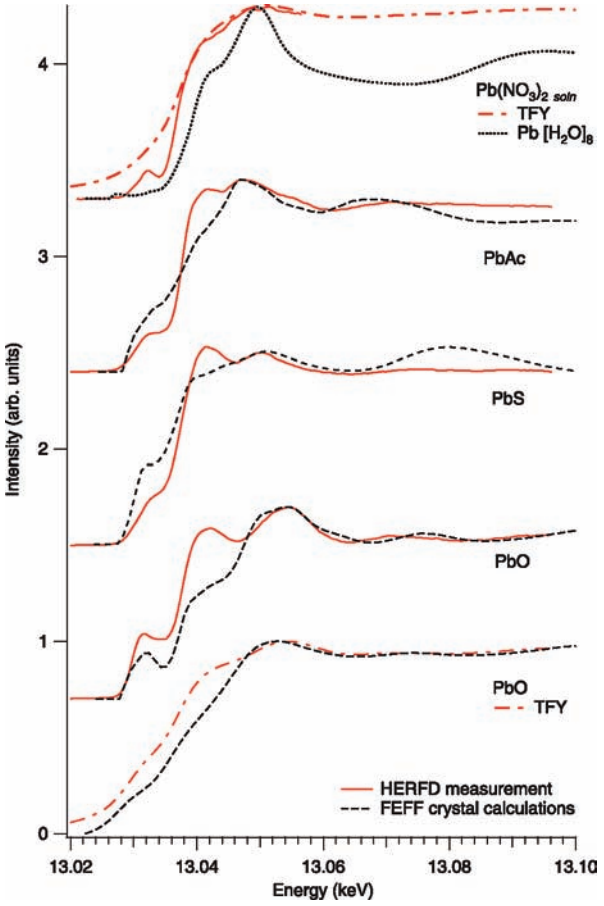

Figure 3. Comparison of measured and FEFF calculated L_3 absorption edge spectra for PbO, PbAc, and PbS solid samples and $Pb(NO_3)_2$ solution. HERFD and standard TFY XANES are shown for PbO to demonstrate the effect of reducing the broadening in FEFF. The TFY spectrum for the $Pb(NO_3)_2$ solution is shown here as the range extends above 13.057 keV. Calculations for an isolated Pb^{2+} ion coordinated with eight water molecules are shown for comparison with the $Pb(NO_3)_2$ solution.

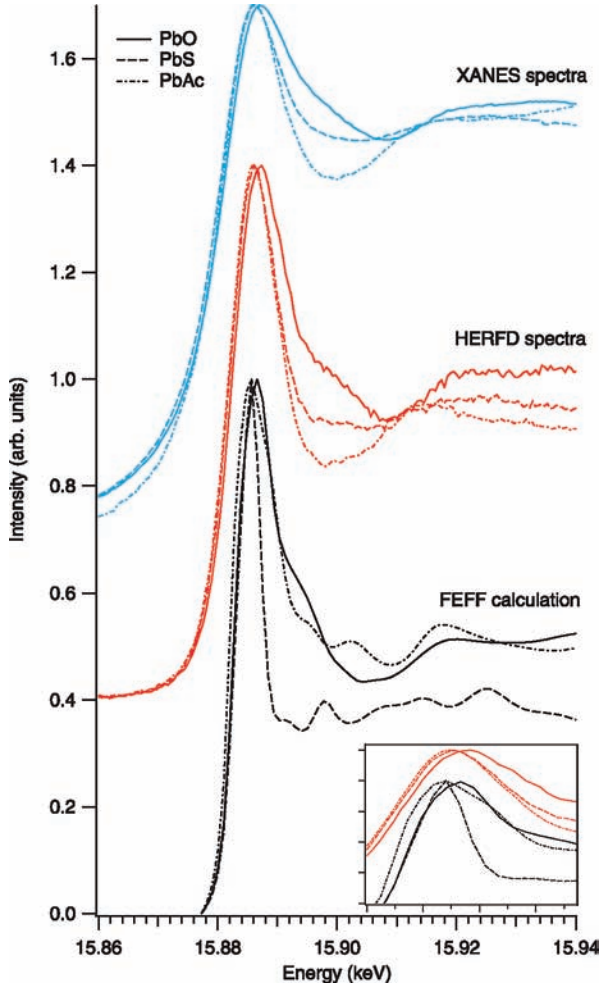

Figure 4. Comparison of measured and reduced broadening calculated spectra for PbO, PbAc, and PbS at the Pb L_1 edge. Inset: Close inspection of the white line peak positions show the peak at higher energy for PbO than for PbS. The edge is also clearly shifted to higher energy for PbO compared with PbS in the HERFD spectra.

normalized at this energy as the maximum intensity generally occurs here) which may be due to self-absorption effects; however, self-absorption does not affect the analysis presented here. The peaks in the TFY XANES spectrum for PbO are broadened in both the experiment and the FEFF calculation, making it a difficult task to confidently identify individual spectral features which are observable in the HERFD spectra.

PbS crystal calculations based on a galena structure reproduce the measured spectral pre-edge feature at 13.033 keV and postedge peaks at 13.041 keV and 13.050 keV, giving a satisfactory calculation of the experimental data.

The PbAc calculations show a feature at 13.030 keV in the pre-edge region, and the measured features at 13.049 keV and 13.071 keV are reproduced. However, there is no obvious sharp absorption edge as seen in the measurements. Thus the differences between the calculated and measured HERFD spectra here may be due to limitations in the theoretical model or the atomic positions used in the calculations. However, this model gives reasonable agreement with the experimental data in terms of pre-edge intensity and peak positions.

Both the HERFD and TFY spectra for $Pb(NO_3)_2$ solution are given, as only the TFY spectrum was recorded above 13.057 keV for solution samples. The spectra show a pre-edge peak at 13.032 keV and postedge peaks at 13.042 keV and 13.050 keV. From previous studies of $Pb(NO_3)_2$ solutions it is known that a high proportion of Pb atoms in $Pb(NO_3)_2$ solution are readily solvated and exist as Pb^{2+} ions bonded to water molecules. Comparison of the $Pb(NO_3)_2$ solution HERFD data with the FEFF calculated spectrum for a Pb^{2+} ion surrounded by eight water molecules shows a reasonable agreement after the absorption edge, although the calculations give a smaller pre-edge intensity to the measured peak at 13.030 keV.

Thus from these examples, we demonstrate that FEFF can be used to satisfactorily calculate experimental L_3 edge HERFD spectra providing the nature of the sample is well understood, i.e. whether the compound can be considered as a crystal as for PbO and PbS, or if predominantly solvated Pb ions are present as with $Pb(NO_3)_2$.

Pb L_1 Edge Measurement and Calculations. The L_1 edge was measured for the powder model samples, PbO, PbS, and PbAc, via standard XANES and HERFD. The spectra are shown in Figure 4 alongside FEFF calculations of the L_1 absorption edge. The calculated broadening for all three compounds was set to −4.2 in the EXCHANGE card. Although the resolution is improved

in HERFD compared with the standard XANES measurements, there is no real increase in spectral detail which can be gained. This is due to the larger final state lifetime broadening of the Lβ_4 line used to measure the L_1 edge, compared with the Lβ_5 line used for HERFD measurements of the L_3 edge. The measured and calculated spectra for PbO exhibit an increased intensity at 15.895 keV compared with the other two samples. This increase in intensity at 15.895 keV for PbO is reproduced by the calculations as is the shift to higher energy of the PbO white line peak. The increased broadening seen in the PbO white line compared to that of PbS is due to the lower symmetry of PbO, which splits the 5*p* levels and gives a broader multicomponent white line compared with that of PbS, which has higher symmetry and lower energy level splitting, and consequently a narrower white line.

A limitation of the FEFF calculation method is seen in the Pb L_1 edge calculations. The input structure for PbAc used is that proposed by Bryant et al.[28] which has a Pb atom coordinated to four oxygen atoms in two acetate molecules, three oxygen atoms from water, and two bridging oxygen atoms (see Figure 1). This structure is similar to that proposed by Wang et al.[7] and Manceau et al.,[10] which have a coordination of Pb with eight oxygen atoms (rather than nine in the Bryant model). The structure used in the calculations here is the best model we have available at present for the PbAc sample, but it may not be accurate enough to reproduce all the spectral features seen in the calculations. Most notably, the white line broadening in the calculated PbAc spectrum is broader than that measured. We suggest this is a consequence of the input model used. FEFF is also known to be more accurate in calculating the absorption spectra for solid state systems than for systems involving organic ligands,[43] which may also play a role in the limited accuracy of the applicability of FEFF in calculating the PbAc spectrum.

FEFF was used to calculate the electron occupation per orbital angular momentum type for the different atoms. In PbS the Pb and S *s* ($l = 0$) orbital angular momenta occupations are both 2.0, with the S *p* ($l = 1$) occupation at 4.1. These figures suggest highly covalent bonding (for a system with no charge donation between atoms, we would expect Pb and S *s* occupations of 2.0 and an S *p* occupation of 4.0). In PbO the Pb and O *s* ($l = 0$) orbital angular momentum occupations are 1.7 and 1.9, respectively, where the O *p* occupation is 4.5, which indicates charge donation between atoms and therefore a more ionic character. These calculated figures are included as an indication of the charge donation and to demonstrate the calculated trend, rather than as absolute values. The shift to higher energy of the white line is observed in Figure 4 for the more ionic PbO with respect to the more covalent PbS and PbAc compounds. The edge and white line peak energies are strongly influenced by screening effects due to the charge density in the valence orbitals. A more ionic system will show a higher energy absorption edge, while additional screening in covalent systems lowers the absorption energy. The reduced background and line-sharpening in the HERFD spectra facilitates identification of this edge shift in the white line peak.

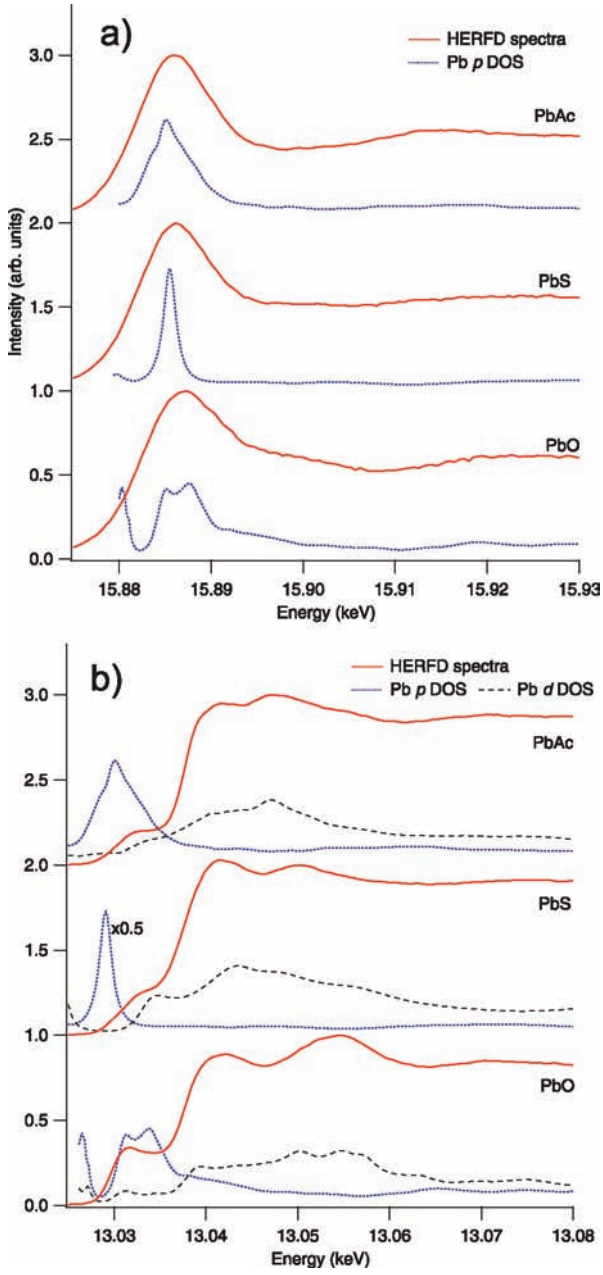

Figure 5. FEFF calculated Pb *p* and *d* DOS for PbO, PbAc, and PbS powder compounds, compared with HERFD spectra (measured and calculated). a) At the Pb L_1 edge the spectrum is predominantly the Pb *p* DOS. b) Past the Pb L_3 absorption edge the spectrum resembles the Pb *d* DOS, but at the pre-edge region (~13.032 keV) there is *p*-*d* orbital mixing for PbO and PbAc giving a stronger pre-edge intensity. The lack of Pb *d* DOS in the pre-edge for PbS means that the pre-edge feature begins at a higher energy than for PbAc or PbO. The Pb *p* DOS for PbS is shown at ×0.5 size for presentation.

Calculated Pb DOS. An examination of the orbital momentum-projected local density of states (*l* DOS) provides detailed information on the origin of the spectral features. The Pb *p* and *d* DOS contributions for the three crystalline model systems were calculated using FEFF and are compared with the measured HERFD spectra at the Pb L_1 and L_3 edges in Figure 5. Comparing the calculated Pb *l* DOS with the measured L_1 absorption edges we see the spectra represent the Pb *p* DOS. The L_1 edge arises from $2s \rightarrow np$, $n \geq 6$ transitions. The sharper calculated white line seen for PbS arises from the single sharp peak in the *p* DOS.

The white lines in PbO and PbAc are broader than for PbS as the Pb *p* DOS is made up of a broader multiple component peak (*vide supra*).

At the L_3 edge we probe $2p_{3/2} \rightarrow nd, n \geq 6$ transitions. Only the PbO and PbAc calculations show a significant calculated pre-edge intensity in the HERFD, where the Pb *p* DOS is a broad multipeak feature coinciding with Pb *d* DOS intensity. This overlap, leading to intensity in the pre-edge of the absorption spectrum, suggests that Pb $p-d$ orbital mixing is present and determines the pre-edge structure. The L_3 HERFD spectrum calculated for PbS does not exhibit a strong pre-edge peak, and PbS has a single sharp Pb *p* DOS peak which does not overlap any Pb *d* DOS intensity in the pre-edge region. Thus only minimal Pb $p-d$ orbital mixing occurs for PbS, and no clear pre-edge peak is seen. Comparing all the calculated L_3 edge HERFD spectra with the Pb *l* DOS beyond the pre-edge region (above 13.035 keV) shows the spectral features to be dominated by the Pb *d* DOS. This is in agreement with similar studies on Pb[37] and Bi[38] compounds where the Pb or Bi *d* DOS was found to dominate the main XANES spectral features after the edge.

We conclude that comparison of the L_1 main edge with the L_3 pre-edge spectra provides valuable information on orbital hybridization where the L_3 pre-edge is only resolved in high-resolution spectra. A mixing of Pb orbitals with *p* and *d* orbital angular momentum is only allowed if no local inversion symmetry with respect to the Pb centers is present. This is the case for strongly distorted PbO and to a lesser extent in PbAc, while PbS exhibits a very high (octahedral) local symmetry. Figure 1 shows the crystal structure for the different compounds. PbO and PbAc have complex structures which lack inversion symmetry with respect to the Pb center; these have a significant pre-edge intensity through *p*-*d* mixing. Galena PbS has a simple cubic type structure with inversion symmetry, which eliminates the ability for *p*-*d* mixing to occur as seen in the lack of a distinct pre-edge. The lack of a clear pre-edge in PbS may also relate to the nature of the ligand and the energy of the outer S *s* electrons.

Contribution of the Ligand DOS. The O and S *s* and *p* DOS were calculated for PbO and PbS and are shown in Figure 6 alongside the Pb *s*, *p*, and *d* DOS and the experimental HERFD spectra. In PbO it can be seen that the O *s* and *p* DOS coincide in energy with the pre-edge peak and also in this case with the Pb *s*, *p* and *d* DOS. Previous DFT studies of the bonding in PbO[39] show that the crystal arrangement has reduced symmetry to drive the hybridization between the Pb *s* and O *p*, Pb *p* and O *p*, and Pb *p* and O *s* DOS, which helps to stabilize the crystal structure. This hybridization argument agrees with our calculations which show the DOS occur at the same energies in the pre-edge region in the O and Pb DOS spectra.

In PbS the S *p* DOS has some intensity coinciding with the Pb *p* DOS, but this is at lower energy than the pre-edge. The first S *s* DOS peak is much lower in energy than the pre-edge. The main contribution to the PbS pre-edge shoulder is the Pb *d* DOS. For PbO we see that the Pb *s*, *p*, and *d* DOS and the O *s* and *p* DOS all coincide at the pre-edge, thus showing that hybridization occurs between these orbitals. We therefore suggest that in PbS the lack in hybridization between the Pb *d* and S *s* and *p* orbitals as evidenced by the calculated DOS explains the weak pre-edge signal at higher energy as compared with PbO. In PbO we see a strong pre-edge due to extensive hybridization between the Pb and O DOS.

Another aspect of the bonding nature of the PbO and PbS systems is the covalency in the system. The FEFF calculations confirm that PbS is less ionic (more covalent) than PbO. We observe that the L_1 white line peak of PbO is shifted to higher energy compared to PbS as expected based on screening arguments. This trend is also seen in

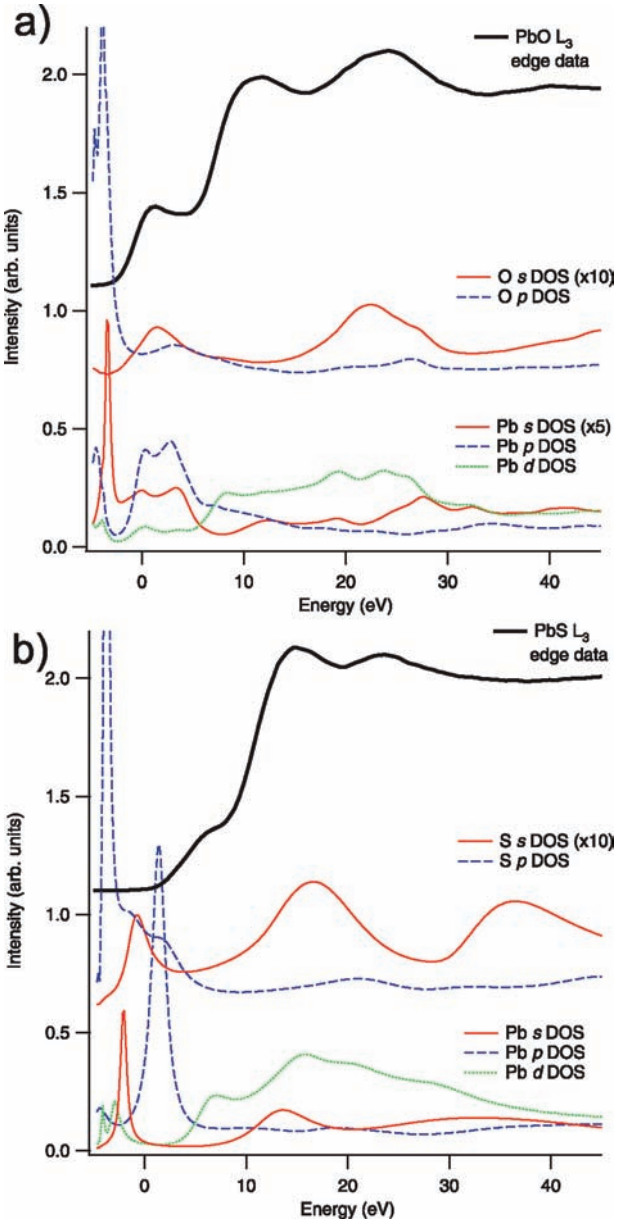

Figure 6. Ligand and Pb DOS calculated in FEFF compared with the measured Pb L_3 edge (shifted so the Fermi level is at 0 eV) for a) PbO and b) PbS. Coinciding intensity between the Pb *s*, *p* and *d* DOS and ligand *s* and ligand *p* DOS indicates hybridization is possible between the orbitals in PbO.

(37) Masterlaro, V. R.; Neves, P. P.; Michalowicz, A.; Eiras, J. E. *J. Phys: Condens. Matter* **2007**, *19*, 226212.
(38) Jiang, N.; Spence, J. C. H. *J. Phys.: Condens. Matter* **2006**, *18*, 8029–8036.
(39) Watson, G. W.; Parker, S. C.; Kresse, G. *Phys. Rev. B: Condens. Matter* **1999**, *59*, 8481–8486.

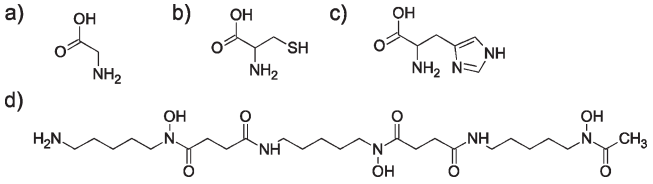

Figure 7. Ligands used in the environmental model Pb samples: a) glycine, b) cysteine, c) histidine, and d) desferrioxamine.

the L_3 main edge position where the edge for PbO is at a higher energy than for PbAc or PbS. However, we see the L_3 pre-edge of PbO at a lower energy than the pre-edge of PbS. This is because the L_3 pre-edge structure is dictated by hybridization effects due to Pb *p-d* orbital mixing, which give the different pre-edge shapes for different samples.

Environmental Model Pb Compounds. Four Pb aqueous model compounds (PbGly, PbCys, PbHist, and PbDFO-B) were included in the study and are shown in Figure 7. The ligands chosen occur at μM levels in natural environments and represent species of interest in inorganic chemistry relating to health physics. Importantly, they also represent possible arrangements of O, N, and S functional groups in naturally occurring macromolecules (e.g., humic substances) which are more abundant and commonly reach mM levels.

Figure 8 shows the HERFD spectra obtained for these Pb compound solutions with the results shown previously for the other model systems. All spectra have been normalized to the most intense measured feature of each spectrum. All spectra exhibit a peak just after the absorption edge at 13.042 keV, although very weakly for $Pb(NO_3)_2$ and PbCys. The two sulfur-containing samples, PbS and PbCys, have the least distinct pre-edge features. The spectra for $Pb(NO_3)_2$, PbHist, and PbDFO-B are very similar to each other. In PbHist and PbDFO-B, we see a precipitate which is likely to contain the Pb complexes, and therefore we conclude the solutions which were measured contained only solvated Pb^{2+} ions. Preliminary EXAFS data and comparison with the FEFF calculations for Pb with eight H_2O molecules support this proposal of solvated Pb^{2+} ions (Figure 3).

The PbGly and PbCys spectra are different to the spectrum of Pb^{2+} ions in solution. PbGly shows a large pre-edge intensity at 13.031 keV and a postedge peak at 13.042 keV. In contrast, the HERFD spectrum of PbCys shows almost no pre-edge peak, and has postedge peaks at 13.042 keV and 13.050 keV. EXAFS data[33] suggest that the PbCys and PbGly species consist of two ligands bonded to Pb to give two ring-like structures, both with very low inversion symmetry. For PbGly Pb−N and Pb−O bonds form, which give two ring structures likely to orient in a hemidirected geometry with an angle of approximately 140−150° between the two rings opposite the Pb lone pair (see Figure 9).

In PbCys, EXAFS analysis shows that Pb−S and Pb−N/O bonds form to give the two ring structures. It is not possible to distinguish whether the second bond is Pb−N or Pb−O; however, Rajh et al. report a Pb-cysteine

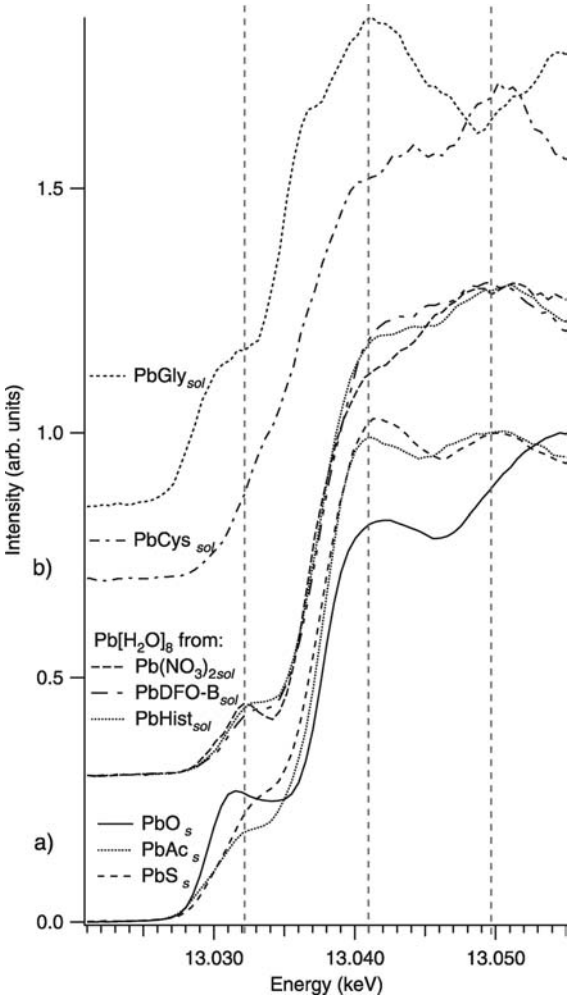

Figure 8. HERFD spectra of all Pb samples. The $Pb(NO_3)_2$, PbDFO-B, and PbHist spectra are very similar to each other, indicating the presence of solvated Pb^{2+} ions. Two solutions, PbGly and PbCys, are different than the other solution samples, suggesting Pb complexes existing in solution. The vertical lines are a guide to relative peak shifts between samples.

structure where the ligand bonds in a bidentate fashion through S and O.[41] In our studies the Pb−S bonds are determined by EXAFS and molecular modeling to be 2.72 Å long, or the Pb−N/O bonds are shorter at 2.43 Å. EXAFS data indicate that the O and N not directly involved in bonding to Pb are oriented to be close to the Pb atom, which is in agreement with early reported measurements which describe a tridentate-fashion bonding between Pb and cysteine O, N, and S atoms.[40] The bond lengths determined by EXAFS are in agreement with other reported structures[14,42] of hemidirected Pb-ligand geometries which occur due to the presence of the Pb lone electron pair. It is also likely that in our samples the Pb atoms are coordinated with a number of water molecules; between two and five coordinations to water are possible from EXAFS fitting and from the possible coordination numbers, which can be up to eight for hemidirected Pb(II) compounds.[14] The EXAFS fitting suggests O/N coordination at a bond distance of 2.71 Å.

(40) Li, N. C.; Manning, R. A. *J. Am. Chem. Soc.* **1955**, *77*, 5225–5228.
(41) Rajh, T.; Ostafin, A. E.; Micic, O. I.; Tiede, D. M.; Thurnauer, M. C. *J. Phys. Chem. B* **1996**, *100*, 4538–4545.
(42) Marandi, F.; Shahbakhsh, N. *Z. Anorg. Allg. Chem.* **2007**, *633*, 11375–1139.
(43) Smolentsev, G.; Soldatov, A. V.; Feiters, M. C. *Phys. Rev. B: Condens. Matter* **2007**, *75*, 144106.

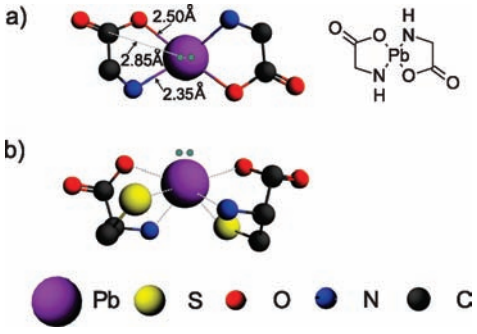

Figure 9. First approximations of the structures of a) PbGly and b) PbCys in solution. The bond distances shown in a) are approximate and have been determined from EXAFS data (Pb−N 2.35 Å, Pb−O 2.50 Å, Pb−C 2.85 Å). The two ring structures are out of plane and are at an angle of ~140° to each other. The structure shown in b) is a possible candidate for the PbCys structure, with hemidirected ligation and bond distances of Pb−S 2.72 Å, a short Pb−O/N distance of 2.43 Å, and a longer Pb−O/N distance of 2.71 Å. Between two and five water molecules (not shown) may be involved in the structure opposite the S atoms. The lone electron pair is indicated on both models.

This contribution may be from the carboxyl-O or amino-N atoms in the organic ligand or from oxygen atoms from additional water molecules. The relatively long Pb−O/N distance may be due to a bond orientation with O positioned closer to the lone electron pair. The models in Figure 9 were obtained using molecular mechanics modeling in ADF[30] to optimize the geometries within the constraints noted above. The additional two to five water molecules bonded to the Pb are omitted for clarity. We stress that these models are first approximations of possible structures.

The HERFD spectra for the two compounds containing S (PbS and PbCys) show similar pre-edge shapes, which are quite different to the pre-edges for non S-containing systems. We conclude that the presence of S close to the Pb atoms (either through the crystal structure in 6-fold coordinated Pb in PbS or the close positioning of S ligand atoms in PbCys) contributes to the characteristic less pronounced pre-edge feature compared with the other Pb systems measured. From the above considerations of the ligand and Pb DOS, the presence of S may influence the Pb *p* DOS intensity so that it occurs below the pre-edge region, thus very little pre-edge intensity is seen in materials or complexes with Pb−S bonding. We can also say that HERFD spectroscopy is a useful complementary technique to EXAFS when deducing atomic positions in complex systems, since we observe a relatively small improvement in the EXAFS spectral fit using different Pb−S/O/N bonding arrangements, but we observe a characteristic pre-edge shape for Pb−S interactions in the HERFD pre-edge compared with Pb−O bonding (comparing PbO and PbS HERFD spectra).

In this study it has been found that molecular complexes are more difficult to reliably model using FEFF than crystalline or solid state materials, and methods which go beyond the muffin-tin approximation may be required for more appropriate modeling.[43] We found that FEFF calculations of the molecular PbGly and PbCys systems cannot be used alone to reliably model the pre-edge features, and comparisons with model systems such as PbS are more instructive.

Conclusion

In this paper we demonstrate that HERFD is a powerful tool in enhancing the spectral features in L_3 absorption edge spectra of Pb compounds through increased resolution by an apparent reduction of the lifetime broadening and that these spectra can be used in chemical speciation studies. HERFD spectra have been compared with FEFF calculations with reduced broadening parameters and agree within the limitations of the calculation method. FEFF was also used to calculate the Pb *l* DOS in the solid model compounds; from an analysis of the Pb *l* DOS we can conclude that the L_3 HERFD spectral shape is governed by Pb *d* DOS where the pre-edge arises from *p*-*d* hybridization. The interpretation is corroborated by the L_1 HERFD spectra that reflect the Pb *p* DOS.

This paper demonstrates that an understanding of Pb model compounds (PbO, PbS, and PbAc) through HERFD measurements and calculations may be used to determine the ligands in more complex Pb compounds. Pb samples which model natural systems by incorporation of amino acid ligands (such as cysteine and glycine) were also measured using HERFD. PbGly and PbCys samples give unique HERFD spectra, and we conclude that these exist as molecular complexes in aqueous solution, most likely as two bidentate ligands per Pb atom bonded through N and O atoms for PbGly and S and either N or O for PbCys. The L_3 pre-edges of PbCys and PbS can be compared and have a characteristic shape which we suggest is due to Pb−S bonding, where the S *s* DOS hybridizes with the Pb *p* DOS below the pre-edge absorption region preventing the possibility of a strong pre-edge peak. Other considerations are the relative positions of the ligand outer *s* electron binding energies and the symmetry of the complex. Using HERFD and FEFF modeling, natural Pb samples from soils or groundwater may be analyzed, and the chemical environment giving rise to particular spectral features can be identified by comparison to the model compounds in this paper and to FEFF calculations.

Acknowledgment. The authors wish to thank the technical support staff at the ESRF. Funding (for U.S. and T.K.) was provided by the Swedish Research Council (contract no. 621-2006-5215) and by ESRF for project EC-320.